Optical properties of zinc selenide clusters from first-principles calculations

Sachin P. Nanavati,[1,2] V. Sundararajan,[1] Shailaja Mahamuni,[3] Vijay Kumar,[4] and S. V. Ghaisas[2,*]
[1]*Centre for Development of Advanced Computing (C-DAC), Pune University Campus, Pune 411 007, India*
[2]*Department of Electronic Science, University of Pune, Pune 411 007, India*
[3]*Department of Physics, University of Pune, Pune 411 007, India*
[4]*Dr. Vijay Kumar Foundation, 1969, Sector 4, Gurgaon 122 001, India*
(Received 17 August 2009; published 14 December 2009)

The optical properties of bare and passivated Zn_nSe_n ($n=1-13$) clusters have been studied within the framework of time-dependent local density approximation. The atomic structure of the clusters has been obtained using projector augmented wave pseudopotential method, with generalized gradient approximation for the exchange-correlation energy. The small clusters with n up to 5 have two-dimensional (2D) structure and for larger sizes, cagelike 3D structures become favorable. At $n=13$, the clusters start getting an atom inside the cage to attain bulklike local structure. For the bare clusters, the highest occupied molecular orbital (HOMO) and lowest unoccupied molecular orbital (LUMO) gap increases from a small value for ZnSe dimer and beyond $n=3$, the variation is small. On the other hand, the HOMO-LUMO gap of the clusters passivated with partially charged hydrogen atom decreases nearly monotonically with increasing size, though the value remains higher compared with that of the bare clusters even for the case of $n=13$. Further, the optical absorption spectra and the corresponding optical gap have been calculated and a decreasing trend as a function of the increasing cluster size has been obtained. This compares well with the experimental results available on larger clusters in the literature though the calculated values underestimate the optical absorption gap as expected within the local density approximation framework.

DOI: 10.1103/PhysRevB.80.245417 PACS number(s): 61.46.Df, 71.15.Mb, 71.15.Dx, 73.22.−f

I. INTRODUCTION

Quantum dots (QDs) of semiconductors have been attracting great attention in recent years due to their possible applications in nanotechnology and miniature devices such as optoelectronics, solar cells, and light-emitting diodes (LEDs).[1] The optical properties of QDs and small clusters are size and shape dependent, besides composition, and therefore, it is possible to tailor these nanomaterials with desired properties. This aspect has led to a large number of studies on II–VI compound clusters, where different colors have been obtained from the same material by changing size and shape, that affect the highest occupied molecular orbital (HOMO)—lowest unoccupied molecular orbital (LUMO) gap due to quantum confinement of electrons. A promising application of such QDs is in their usage as a fluorescent marker to provide information about a biological state or event.[2] They have remarkable advantages as compared to the traditional organic dyes, *viz.*, broad absorption with narrow and symmetric photoluminescence (PL) spectra, high resistance to photobleaching and exceptional resistance to photo and chemical degradation.[3] They can be observed and tracked over an extended period of time (up to few hours) *in vivo* imaging and diagnostics of live cells.[4] Therefore, developing an understanding of the properties of such systems is an area of wide interest, not only in semiconductor physics, but also from biological systems point of view.

Among the II–VI compound semiconductors, QDs of ZnSe have several technological advantages and have been actively studied. This environment friendly material is one of the leading candidates for the fabrication of blue LEDs and laser diodes.[5] Experimentally, highly monodisperse ZnSe nanoparticles have been prepared through chemical route treatment.[5,6] Recently, ZnSe/ZnS core/shell nanoparticles have shown a spectacular increase in the PL quantum efficiency from 2% to 42%, in their spectra.[7]

From a theoretical point of view, most studies have been done on small clusters because one needs to find the ground state structure of clusters that are often very different from the bulk. As the size grows, it becomes challenging to find the lowest energy structure of clusters and so far, most of the first principles studies on semiconductor clusters are on systems having up to about 50 atoms. In the case of ZnSe, small Zn_nSe_n ($n=1-9$) clusters have been studied earlier by Matxain *et al.*,[8] who calculated the ground state geometries and cohesive energies using B3LYP gradient-corrected density-functional method with GAUSSIAN98 package. Deglmann *et al.*,[9] have obtained the atomic structures of ZnSe clusters up to heptamers ($n=7$). Recently, Goswami *et al.*[10,11] have calculated the structural and electronic properties of unpassivated, Zn_mSe_n ($m+n\sim 200$) clusters using density functional tight-binding (DFTB) method within the local density approximation (LDA). The excitation spectrum was calculated using time-dependent (TD) density functional response theory (DFRT) within the tight-binding approach. They considered initial structure as spherical parts of either zinc blende or wurtzite crystal structure. The stoichiometric Zn_nSe_n clusters were also passivated by terminating the dangling bonds on the surface by either -H or -OH. However, as mentioned before, the ground-state structure of small clusters is expected to be different from the bulk. Therefore, determination of the atomic structures using a parameter free, first principles method is important for understanding the properties of semiconductor clusters. In the present work, we investigate the structure of small bare as well as surface passivated Zn_nSe_n ($n=1-13$) clusters with partially charged hydrogen and report their optical absorption spectra.

The rest of the paper is organized as follows: in Sec.II, we present the details of the computational methodology and in Sec.III, the results of the structural and optical properties of the bare and passivated clusters are given. Section IV summarizes the results of the present study.

II. COMPUTATIONAL METHODOLOGY

The atomic structure and optical spectra of $(ZnSe)_n$ $(n=1-13)$ clusters have been studied in a two step procedure. (i) A few initial geometries were optimized to the nearest minima, within the framework of pseudopotential based Kohn-Sham density functional theory (DFT) and the lowest energy isomers of clusters and their electronic structure were determined. (ii) The optical spectra of the optimized structure were calculated within TD-LDA, for both the bare and the passivated clusters.

The first part (optimization of the structures) of the calculations has been carried out using VASP package,[12,13] with projector augmented wave (PAW) method[14,15] and generalized gradient approximation (GGA) for the exchange-correlation energy.[16] This approach is known to provide good atomic structure of many semiconductor clusters. The valence configuration of Zn and Se were taken to be $3d^{10}$ $4s^2$ and $4s^2$ $4p^4$, respectively. The cutoff energy (E_{cut}) for the plane wave expansion is set to 276.7 eV. The clusters are placed within a cubic supercell such that the distance between the outermost atom in the cluster and the simulation box boundary is at least 6 Å. Such a large box is sufficient to keep the interaction between the cluster and its periodic images to be negligibly small. The clusters are relaxed using preconditioned conjugate gradient (CG) method.[17] The convergence criteria for energy and forces were ~0.0001 eV and ~0.004 eV/Å, respectively. The optimized atomic structures of the bare CdSe clusters[18] were used as the starting structure of ZnSe clusters. Generally, it has been observed that clusters of II–VI semiconductors exhibit similar geometries as evident in the case of CdTe clusters.[19,20] After optimization, ZnSe clusters were passivated with partially charged fictitious hydrogen atoms (H^*),[21] in a manner that their surfaces remained electronically neutral. For a II–VI type semiconductor like ZnSe, a H^* of $z=1.5e$ (e =electronic charge) is attached to Zn atoms, while a H^* of $z=0.5e$ is attached to a Se atom, to maintain overall charge neutrality and tetrahedral coordination around each atom. These structures are reoptimized to obtain the final geometry of passivated cluster.

In the next step, the optical spectra of the optimized bare and passivated clusters are calculated using a *real* space formalism. For this, initially a static calculation of the wave function optimization is performed for the optimized geometry of the clusters within the DFT formalism, using PARSEC code[22,23] and norm-conserving Troullier-Martins pseudopotentials.[24] The exchange-correlation energy has been calculated within LDA using the Ceperley-Alder data[25] with Perdew-Zunger parametrization.[26] The optimized charge density and the corresponding electronic states serve as an input to the TD-DFT method based on TD-LDA,[27,28] to obtain the optical absorption spectrum.

In the real space formalism, the wave functions are not decomposed into any basis set, rather a three-dimensional (3D) grid is constructed around the center of the cluster which is enclosed by a sphere of sufficient radius, R_{max}, such that the wave functions approach zero value on its surface. The Kohn-Sham equations are then directly solved at each grid point by expanding the kinetic energy part using a higher order finite difference method.[29] The grid spacing, h, is important for the accuracy of the calculations and it plays a similar role as the cut-off energy in the plane wave expansion. In the present calculations, h is kept in the range of 0.21–0.26 Å, while R_{max} is ~2.11–3.17 Å, farther than the outermost atom in the cluster. For calculating the optical spectra, the wave function is further optimized using R_{max} ~5.3–6.35 Å, greater than the farthest atom in the cluster and with the number of unoccupied states more than double that of the occupied ones.

III. RESULTS

In this section, we present the results of the atomic and electronic structure of the bare and passivated clusters as well as their optical absorption spectra.

A. Atomic structure of bare clusters

The optimized atomic structures of the bare Zn_nSe_n clusters with $n=2$ to 13 are shown in Fig. 1. It is observed that clusters with $n=2$ to 4 are planar (or nearly planar). For Zn_2Se_2, a four-membered ring forms a parallelogram with two Se atoms at the opposite ends of a Zn dimer. Zn_3Se_3 forms a six-membered ring and it could be considered as a bent triangle with Se atoms occupying its three corners, while Zn atoms are placed at positions slightly displaced from the center of each side. This stable ring forms the basis of most of the larger clusters. Zn_4Se_4 forms a twisted rhombus with Se atoms at the vertices as shown in the figure. The Zn atoms again occupy positions near the center of the edges. For $n=5$, a buckled pentagon with a ring structure lies lowest in energy. The Se atoms lie at the vertices of the pentagon while Zn atoms are placed around the center of the edges. Beyond $n=5$, 3D structures become most favorable.

Zn_6Se_6 has a 3D structure formed by stacking of two six-membered rings (Zn_3Se_3), one above the other but rotated with respect to each other such that Zn atom is neighbor to Se and vice-versa. In the optimized structure, the six-membered ring becomes nonplanar with Se atoms slightly pulled outward while Zn atoms are pulled inward, so that, the bonding develops some sp^3 character. Zn_7Se_7 has two nearly degenerate isomers. One isomer is a capped structure [Fig. 1(g)], formed by three interlinked six-membered rings, with three-sided rubylike structure in a threefold symmetric fashion. Each six-membered ring is connected to the two remaining six-membered rings via ZnSe bonds. The seventh Se and Zn atoms cap opposite faces of this structure along the symmetry axis. The second isomer [Fig. 1(f)] is obtained by adding one ZnSe unit to the Zn_6Se_6 structure on its side. For further analysis, we have used this structure, as larger clusters could be built using this isomer. Zn_8Se_8-I [Fig. 1(h)],

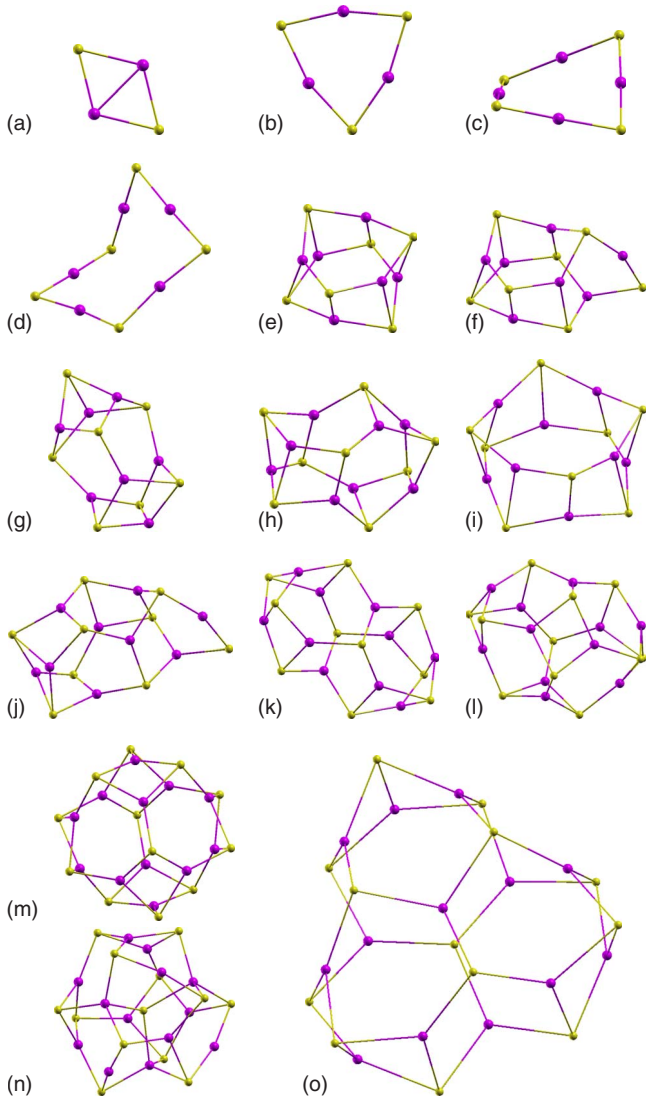

FIG. 1. (Color online) (a)–(o) show the optimized atomic structures of the bare Zn_nSe_n (n=2–13) clusters. The dark balls (pink online) represent Zn while the light gray balls (yellow online) represent Se atom. (f) and (g) are nearly degenerate isomers of n = 7, (h) and (i) correspond to n = 8 with the former having the lowest energy, while (n) and (o) are isomers of n = 13 cluster. (n) has the lowest energy and (o) has been obtained from optimization of a bulk fragment.

is composed of two stacked six-membered rings, which are buckled and joined with a four-membered ring. This structure lies ~0.12 eV lower in energy than an isomer with two eight-membered rings (Zn_4Se_4) stacked one above the other [Fig. 1(i)] and rotated with respect to each other to have Zn (Se) as neighbor to Se (Zn). Zn_9Se_9 is similar to Zn_8Se_8 with an additional ZnSe dimer attached to its one end. All these 3D structures are cagelike with six and four-membered rings. The cagelike elongated $Zn_{10}Se_{10}$ structure is composed of two Zn_6Se_6 units fused together by a pair of ZnSe bond. $Zn_{11}Se_{11}$ forms a structure by the combination of six-membered and four-membered rings. Maintaining this trend, $Zn_{12}Se_{12}$ forms a symmetric, closed, cubic hollow cage structure made up of eight six-membered and six four-membered rings. On the other hand, $Zn_{13}Se_{13}$ forms a closed shell structure made up of buckled four- and six-membered rings as in the case of n=12, but with a Se atom occupying the shell center and forming 4 bonds with the surface Zn atoms. The distance between the Se atom at the center of the cage and three surface Zn atoms is 2.51 Å, while the remaining bond with the fourth Zn atom is 2.64 Å. There are three Zn atoms, which form only two bonds with their neighboring Se atoms. The overall symmetry of the shell gets reduced as compared to $Zn_{12}Se_{12}$ cage. Further, a bulklike geometry for n=13 is optimized [Fig. 1(o)], referred as $Zn_{13}Se_{13}$-II, in which three six-membered rings, each having two common bonds with the neighboring rings and a common Zn atom, are placed on another similar structure but with a common Se atom such that, Zn (Se) have Se (Zn) as nearest neighbors. This structure lies ~0.624 eV higher in energy than the above discussed isomer. In all the 3D structures discussed above, Se atoms try to come out of the plane (cage) as compared to Zn atoms.

The physical properties of the lowest energy isomers have been calculated and Table I summarizes the binding energy E_b, Zn-Se nearest neighbor bond length b_l, HOMO-LUMO gap E_g, and ∠(Se-Zn-Se) for the bare clusters. For the cases of n=1 to 5, we have calculated the average values of b_l and ∠(Se-Zn-Se), while for the remaining clusters, the minimum and the maximum values in their variations are shown. Further, the calculated values are compared with those available in the existing literature[8] for $n \leq 9$ (except for n=7, in which case our geometry is different from the reported one) and generally the agreement is good. The ∠(Se-Zn-Se) is larger for atoms which are part of a six-membered ring as compared to that of a four-membered one.

B. Atomic structure of passivated clusters

The optimized atomic structures of the passivated clusters are shown in Fig. 2. As mentioned earlier, ZnSe clusters are passivated with partially charged, fictitious hydrogen atoms (H^*), to saturate the surface dangling bonds. Such a passivation scheme results in each Zn and Se atom to have four nearest neighbors. This leads to stoichiometries of $ZnSeH_6^*$ for n=1, $ZnSeH_4^*$ for n=2–5 (planar or nearly planar structures), and $ZnSeH_2^*$ for 3D structures. There are a few exceptions in the case of the 3D clusters, such as n=7, 9 and 13, due to the presence of twofold coordinated Zn and Se atoms in the bare clusters. Also for n=13 isomer I, there is a Se atom at the center and four Zn atoms at the surface that are already fourfold coordinated and therefore, no addition of H^* is required for them. In general, the passivation enforces a more symmetric structure with tetrahedral bonding (Se-Zn-Se bond angles lying approximately in the range of 95–120°) around each atom. There is an increase in the average Zn-Se bond length, b_l (except for the case of n=2) and the HOMO-LUMO gap, E_g as it can be seen from Table II.

The passivation of a cluster by H^* can be viewed to have an effect of creating bulklike environment on the surface of the clusters. Bulk ZnSe has zinc blende structure with ∠(Se-Zn-Se)=109.4° and b_l=2.454 Å. With passivation, the clusters tend to form a part of the bulk within the given

TABLE I. Binding energy E_b (eV/atom), range of the nearest-neighbor Zn-Se bond lengths, b_l (Å), HOMO-LUMO gap, E_g (eV), and the angle Se-Zn-Se (degree) of the bare ZnSe clusters. Values given within brackets are taken from Matxain *et al.*[8]

Clusters	E_b	b_l	E_g	∠(Se-Zn-Se)
ZnSe	0.72	2.17 (2.2)	0.45	
Zn_2Se_2	1.69	2.58 (2.38)	1.52	113.56 (116.8)
Zn_3Se_3	2.10	2.30 (2.32)	2.73	162.53 (160.4)
Zn_4Se_4	2.17	2.28 (2.30)	2.96	178.26 (177.9)
Zn_5Se_5	2.17	2.28 (2.30)	3.04	172.42–178.35 (172.2–178.5)
Zn_6Se_6	2.19	2.40–2.56 (2.43–2.59)	2.29	104.07–141.56 (103.4–141.1)
Zn_7Se_7-I	2.26	2.39–2.48	2.37	102–18–133.62
Zn_7Se_7-II	2.26	2.25–2.56	2.05	102.26–159.46
Zn_8Se_8-I	2.32	2.38–2.52 (2.41–2.51)	2.49	102.28–139.2 (102–139.3)
Zn_9Se_9	2.31	2.38–2.52 (2.40–2.50)	2.15	101.67–137.81 (101.7128.9)
$Zn_{10}Se_{10}$	2.34	2.39–2.54	2.40	102.17–137.11
$Zn_{11}Se_{11}$	2.37	2.38–2.50	2.51	101.32–130.9
$Zn_{12}Se_{12}$	2.40	2.36–2.45	2.73	99.4–130.4
$Zn_{13}Se_{13}$-I	2.39	2.39–2.70	2.78	98.26–166.34
$Zn_{13}Se_{13}$-II	2.37	2.39–2.51	2.58	103.01–141.4

degrees of freedom. Table II shows that the bond angles are close to the bulk value with less variations, confirming the effect of passivation. The deviations from the bulk structure of ZnSe cluster is due to the presence of dangling bonds in bare clusters because of the finite size, which might also lead to a reconstruction and in the case of small clusters, often a complete transformation of the structure with a possible change in the bonding character as well. With passivation depending upon the species, one can recover local tetrahedral bonding character, as in the present case. For the bulklike isomer of $n=13$ [isomer II in Fig. 2(p)], the passivation effect is evident as the variation from the bulk value of the bond length and bond angle is less. Also, this structure is about ~0.04 eV lower in energy than the one obtained from the passivation of the lowest energy bare cluster [Fig. 2(o)], indicating that the passivation makes bulklike environment slightly more favorable, even for such small clusters.

C. Physical properties

The total densities of states (DOS) for the bare and passivated clusters, in a few selected cases, *viz.*, $n=1$, 6, and 12, are shown in Fig. 3. The plots show that for the bare clusters, electronic states arising from the Se 4*s* orbital lie deep inside the electronic spectra followed by the Zn 3*d* states. The occupied states near the HOMO level are predominantly Se 4*p* type. In between the Zn 3*d* and Se 4*p* states, there is a hybridization of Zn 4*s* state, primarily with the 4*p* states of Se. These features remain nearly the same in all clusters, except that there is a broadening of the corresponding distribution of states as n increases. For ZnSe ($n=1$), the HOMO-LUMO gap is small and the LUMO state arises from hybridization of Zn 4*s* and 4*p* states with the Se 4*p* states. Other unoccupied states near the LUMO have mainly Zn 4*p* character. For larger clusters the HOMO-LUMO gap is quite significant and it is given in Table I. It can be seen that the cluster with $n=5$, has the largest HOMO-LUMO gap, even though it does not have high structural symmetry. Also, the HOMO-LUMO gap is large for $n=13$ cluster, though in this size range, the cluster with $n=12$ has the highest symmetry.

In the case of the passivated clusters, the DOS gets modified due to the presence of the additional levels of the fictitious H^* atoms and their hybridization with the states of the ZnSe clusters. As it can be seen from Fig. 3 that for $ZnSeH_6^*$, the states derived from Se 4*s* level remain at around the same energy as that of the bare cluster, but with a small shift to the lower binding energies. The *s* orbital states of three H^* atoms with $z=1.5e$, lie between Se 4*s* and Zn 3*d* states, but close to the latter. These three H^* states, hybridize with the 4*s* and 3*d* states of Zn. One of these states has stronger hybridization with the 4*s* state of Zn while the other two have strong hybridization with the Zn 3*d* states. The state lying at around −4 eV is composed mostly of Zn 3*d*. The next two states also have strong hybridization between the *s* states of H^* atoms with $z=1.5e$ and the 3*d* states of Zn. The last three occupied states near the HOMO arise from the 4*p* states of Se that hybridize with the *s* states of $3H^*$ atoms with $z=0.5e$, as well as with the 4*s*, 4*p*, and 3*d* states of Zn. The HOMO-LUMO gap of the passivated clusters becomes much larger compared with the bare clusters. Similar features are seen in the electronic spectra of larger passivated clusters. It is to be noted that the electronic spectrum of $n=12$ cage cluster, is sharper as compared to the spectrum of the $n=6$, as the former cluster has higher symmetry.

Figure 4 depicts the probability charge density of the HOMO and the LUMO states of the bare and passivated clusters, for $n=6$ and 12 cases. The HOMO of the bare clusters arises predominantly from Se 4*p* states with a scanty charge on Zn atoms. Passivation retains these features and the Se 4*p* orbital features can be seen in the HOMO plot. The

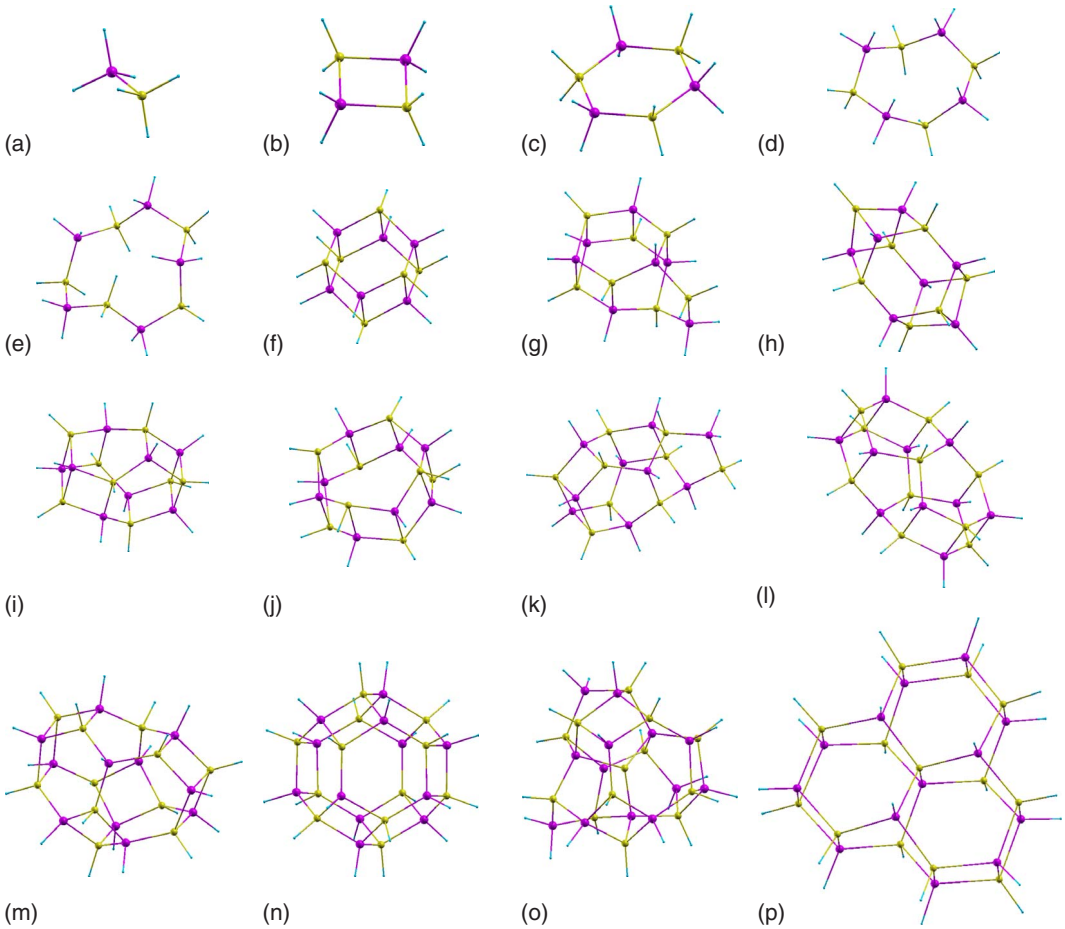

FIG. 2. (Color online) Optimized atomic structures of the passivated Zn_nSe_n ($n=1-13$) clusters. The dark balls (pink online) represent Zn, the light gray balls (yellow online) are Se, while the small light gray balls (blue online) show partially charged fictitious H^* atoms. The sequence of the structure is similar to that in Fig. 1, but shifted due to the addition of $ZnSeH_6^*$ in (a).

LUMO of the bare $n=6$ cluster [Fig. 4(e)], shows hybridization of $4p$ and $4s$ orbitals of Zn with some orbital distribution in the interstitial region. However, the situation is totally different once passivated [Fig. 4(f)]. Now, the LUMO arises from the hybridization of Se $4s$ and $4p$, Zn $4s$ and $4p$ as well as both the types of H^* s orbitals. Also, as observed in the bare case, there is a significant distribution in the interstitial region between the two hexagonal rings. Similar observation is found in the case of the LUMO of both the bare and the passivated $n=12$ clusters, except for the distribution in the cage.

A comparison between the variation in the HOMO-LUMO gap (E_g) of the bare and passivated clusters [Fig. 5(a)] shows that there is a significant increase in the energy gap upon passivation. This increase in the gap is because of the removal of the localized states arising from the surface dangling bonds, from the region near the HOMO to higher binding energies. Because of this, the HOMO-LUMO gap widens upon passivation. Further in contrast to the bare clusters, the HOMO-LUMO gap of the passivated clusters shows a nearly continuous decrease as the size increases, with the largest value for $ZnSeH_6^*$ (see Table II). The HOMO-LUMO gap has a locally maximum value for $n=3$ and 12, both of which have relatively high symmetry.

TABLE II. Binding Energy, E_b (eV/atom), range of the nearest-neighbor Zn-Se bond lengths, b_l (Å), HOMO-LUMO gap, E_g (eV), and the angle Se-Zn-Se (degree) of the passivated ZnSe clusters.

Clusters	E_b	b_l	E_g	∠(Se-Zn-Se)
$ZnSeH_6^*$	2.29	2.41	6.04	
$Zn_2Se_2H_8^*$	2.30	2.47	5.18	94.32
$Zn_3Se_3H_{12}^*$	2.60	2.44	5.21	119.34
$Zn_4Se_4H_{16}^*$	2.33	2.44	4.96	114.09–115.29
$Zn_5Se_5H_{20}^*$	2.33	2.45	4.90	112.58–115.34
$Zn_6Se_6H_{12}^*$	2.34	2.46–2.61	4.26	109.47–111.60
$Zn_7Se_7H_{16}^*$-I	2.35	2.44–2.49	4.02	97.33–116.05
$Zn_7Se_7H_{14}^*$-II	2.34	2.46–2.50	4.06	95.76–114.75
$Zn_8Se_8H_{16}^*$-I	2.36	2.43–2.51	3.97	95.21–117.42
$Zn_9Se_9H_{20}^*$	2.36	2.43–2.49	3.97	95.48–116.23
$Zn_{10}Se_{10}H_{20}^*$	2.35	2.45–2.52	3.78	95.8–118.19
$Zn_{11}Se_{11}H_{22}^*$	2.36	2.43–2.52	3.88	94.38–119.33
$Zn_{12}Se_{12}H_{24}^*$	2.36	2.43–2.50	4.00	93.08–120.52
$Zn_{13}Se_{13}H_{24}^*$-I	2.37	2.44–2.64	3.56	94.43–119.72
$Zn_{13}Se_{13}H_{24}^*$-II	2.37	2.46–2.51	3.72	96.13–115.75

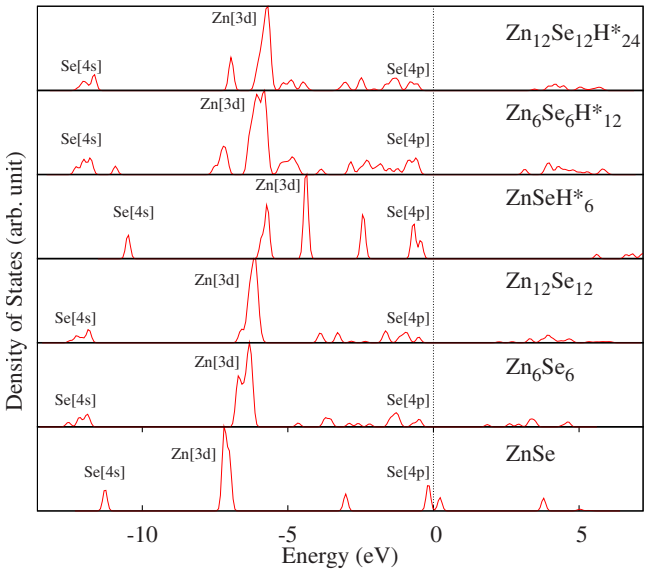

FIG. 3. (Color online) Density of states (DOS) of the bare and the passivated $(ZnSe)_n$, $n=1$, 6, and 12 clusters. In all the above cases, the HOMO is shifted to 0 eV and the DOS is smeared with a Gaussian of standard deviation 0.1 eV.

The trend in the binding energy (BE) per atom (E_b) for both the bare and the passivated clusters is shown in Fig. 5(b), and the values are given in Table I and Table II. For the bare and the passivated clusters, E_b was calculated as follows:

$$E_b^{\text{bare}} = \frac{nE_{\text{Zn}} + nE_{\text{Se}} - \text{Zn}_n\text{Se}_n}{2n} \tag{1}$$

$$E_b^{\text{pass}} = \frac{nE_{\text{Zn}} + nE_{\text{Se}} + mE_{\text{H}^*}^{1.5} + mE_{\text{H}^*}^{0.5} - \text{Zn}_n\text{Se}_n\text{H}_{2m}^*}{2(n+m)}, \tag{2}$$

where E_{Zn}, E_{Se}, $E_{\text{H}^*}^{1.5}$, and $E_{\text{H}^*}^{0.5}$ are the energies of Zn, Se, $H^*(z=1.5e)$ and $H^*(z=0.5e)$ atoms, respectively. The BE of the bare clusters increases with the size. The passivation increases the BE of the small clusters and up to $n=10$, it is higher as compared to the value for the bare clusters. For $n=11$ and 12, the BE of the bare clusters is higher than the values for the passivated counterparts by 0.01 and 0.04 eV/atom, respectively. Among the passivated clusters, $n=3$ has larger BE and hence is more stable. Further, a comparison of the values of E_b of the bare clusters with those reported in the literature using GAUSSIAN package,[8] shows that the BE/atom calculated by GGA with VASP package is on the higher side, but the overall trend is similar.

The optical spectra have been calculated within the TD-LDA formalism for the bare and the passivated clusters. The first optical absorption gap is defined as the energy of the first allowed dipole transition. But usually this criterion is impractical since the intensity of the first allowed transition could be extremely weak depending upon the oscillator strength. Hence, an *effective* optical gap, $\Omega_g(p)$, is calculated using a certain cutoff value[27] defined as

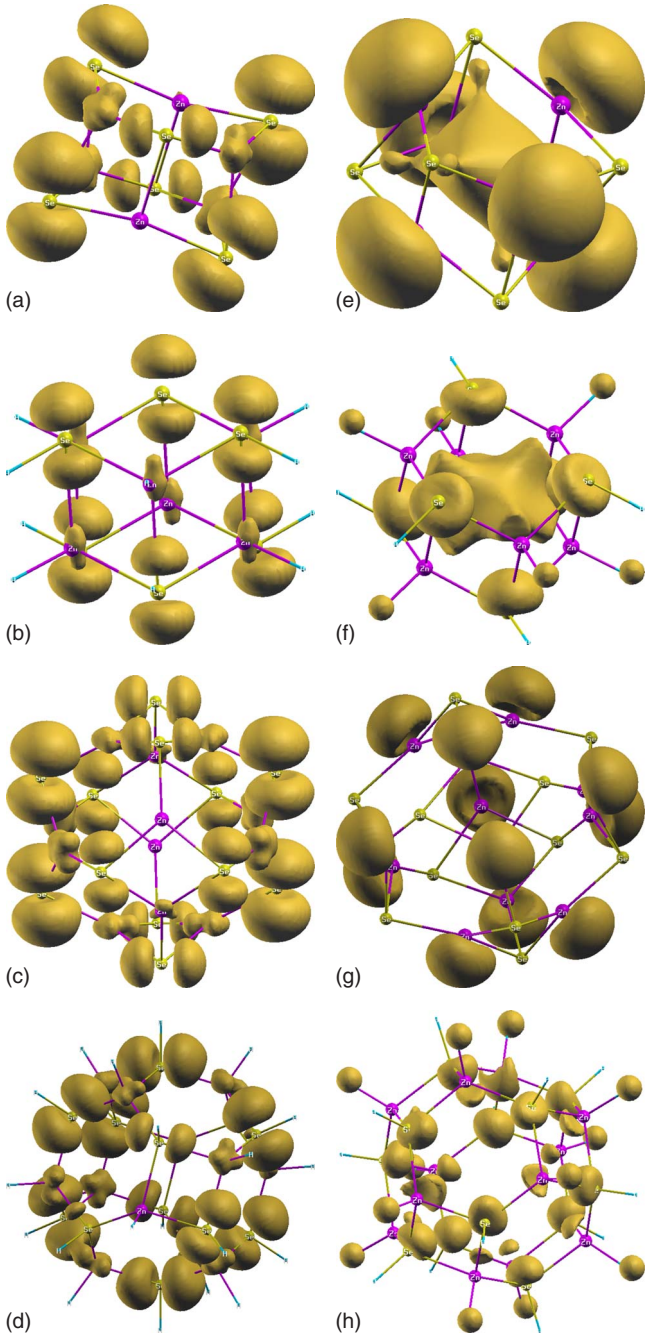

FIG. 4. (Color online) Isosurfaces of the HOMO for (a) bare, $n=6$, (b) passivated, $n=6$, (c) bare, $n=12$, and (d) passivated, $n=12$ clusters. The corresponding isosurface of the LUMO is shown in (e)–(h), respectively.

$$\int_0^{\Omega_g(p)} \sigma(\omega)d\omega = pf_e, \tag{3}$$

where $\sigma(\omega)$ is the photoabsorption cross-section per electron, f_e is the complete one electron oscillator strength defined as, $f_e = 2\pi^2\hbar e^2/mc \sim 1.098$ eV Å^2 and p is a small positive number whose value is taken as 0.02.

The optical gap calculated according to the above formula is shown in Fig. 6(a). A comparison of the optical gap for the

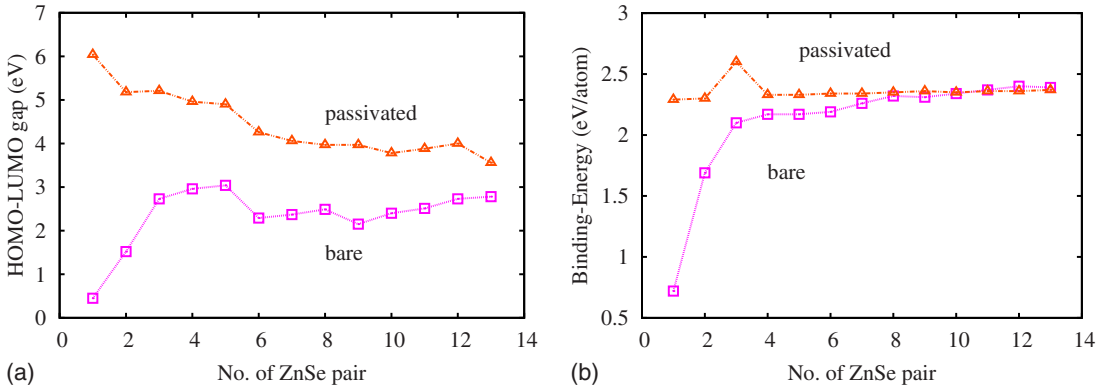

FIG. 5. (Color online) The variation of (a) the HOMO-LUMO gap (E_g) and (b) the binding energy, for both the bare and the passivated ZnSe clusters. In all the cases, calculations were performed using PAW pseudopotentials with the GGA exchange-correlation functional.

bare and the passivated clusters shows that, in most cases, passivation increases the gap significantly. But for $n=2$, the change is insignificant, while for $n=3$ and 13, the gaps of the bare clusters are larger by 0.09 and 0.28 eV, respectively, as compared to the values for their passivated clusters.

It is to be noted that experimentally, the size estimation of the passivated ZnSe QD is carried out by using x-ray diffraction (XRD) and transmission electron microscopy (TEM) technique. The XRD technique determines the size of the crystalline core, while TEM measures the size of the core along with the organic capping agent. In the present calculation, the size of a passivated cluster is determined by taking the largest distance between any pair of atoms, excluding H^*, in order to compare with the XRD data. The largest size among the calculated clusters is that of $Zn_9Se_9H^*_{20}$, 9.4 Å due to its elongated structure, with an optical gap of 4.14 eV (Table III). At the same time, the experimental values of the smallest QD size and the optical gap are, respectively, 15 ± 3 Å and 3.89 eV.[6] In Fig. 6(b), the optical gap obtained from both calculation and experiment, is plotted with increasing cluster size. There is a decreasing trend of the gap with increasing size and our results show that the calculated optical gap is smaller than the observed one. This is expected since the LDA calculations are known to underestimate the HOMO-LUMO gap and hence the value of the optical absorption gap.

The TD-LDA optical absorption spectra of the bare and the passivated clusters are shown in Figs. 7 and 8, for all the cases. For the bare clusters, there are small peaks in the low energy region corresponding to the unsaturated surface bonds. Once passivated, the corresponding electronic states get shifted to the higher energy side. Further, in most of the passivated cases (except for $n=6$, 7, and 8), the optical gap calculated by 2% cutoff, nearly matches with that of the first peak. In general, the spectra of the symmetric passivated clusters (like $n=2$ and 12) in the low energy range are better resolved, as compared to the less symmetric clusters (such as $n=13$ isomer I), with respect to the separation in their first and second peak. The optical absorption spectrum of the passivated bulk fragment has more features as compared to the one obtained from the best structure of the bare $n=13$ cluster. Since, energetically the two isomers are nearly degenerate, measurement of the optical absorption spectra could suggest the kind of isomers present in the sample.

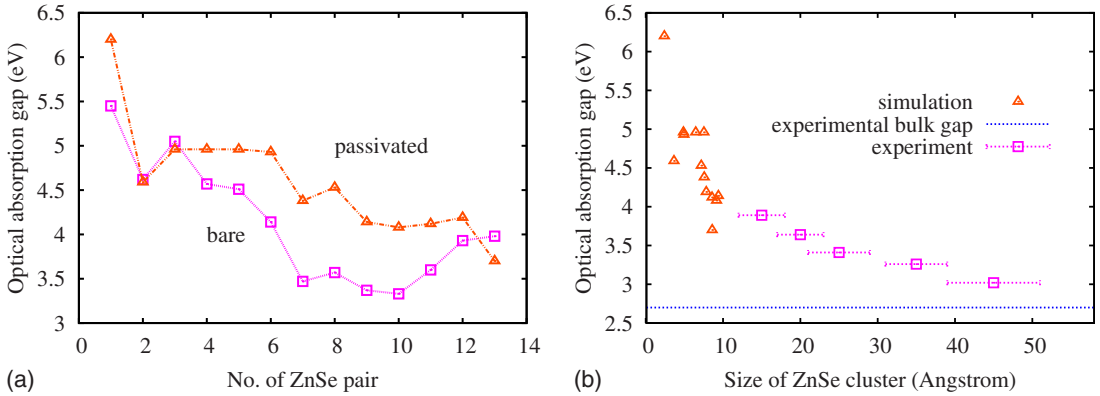

FIG. 6. (Color online) The optical absorption gap of Zn_nSe_n ($n=1-13$) clusters calculated by Eq. (3). (a) shows the calculated optical absorption gap for the bare (squares) and the passivated (triangles) clusters with increasing number of ZnSe pair. These gaps were calculated using Troullier-Martins pseudopotentials within the TD-LDA formalism. In (b), the same optical gap is plotted as a function of the increasing cluster diameter for the passivated case. The triangles represent the calculated gap, while the square boxes correspond to the experimental result obtained by capping the ZnSe quantum dot with organic passivating agents (Ref. 6). The horizontal line at 2.7 eV represents the experimentally obtained bulk optical gap.

TABLE III. Cluster size (maximum distance between Zn and Se atom) and the corresponding calculated optical absorption gap of the passivated cluster.

Cluster	Size (Å)	Optical gap (eV)
$ZnSeH_6^*$	2.41	6.20
$Zn_2Se_2H_8^*$	3.65	4.59
$Zn_3Se_3H_{12}^*$	4.88	4.96
$Zn_4Se_4H_{16}^*$	6.47	4.96
$Zn_5Se_5H_{20}^*$	7.53	4.96
$Zn_6Se_6H_{12}^*$	4.94	4.93
$Zn_7Se_7H_{16}^*$-I	7.57	4.38
$Zn_8Se_8H_{16}^*$	7.18	4.53
$Zn_9Se_9H_{20}^*$	9.40	4.14
$Zn_{10}Se_{10}H_{20}^*$	9.16	4.08
$Zn_{11}Se_{11}H_{22}^*$	8.58	4.12
$Zn_{12}Se_{12}H_{24}^*$	7.83	4.19
$Zn_{13}Se_{13}H_{24}^*$-I	8.60	3.70
$Zn_{13}Se_{13}H_{24}^*$-II	9.04	3.88

IV. CONCLUSION

We have presented the results of the atomic structure of the bare and the passivated Zn_nSe_n ($n=1-13$) clusters and their optical absorption spectra obtained from first principles calculations. The optimized geometries show that for $n>5$, there is a structural transition from 2D to 3D clusters and cagelike structures are energetically most favorable. There is a corresponding change in the coordination number from two to three, till $n=12$, which has a high-symmetry cage structure. For $n=13$, there is a Se atom inside the cage and the coordination number four begins to show up, indicating initialization of the bulklike structure. Surface passivation with fictitious H^* atoms provide a bulklike environment due to the formation of tetrahedral coordination. This is reflected in the values of the bond lengths and bond angles which tend to achieve bulk values. Also the passivated bulk fragments, are nearly degenerate with those obtained from the passivation of the lowest energy isomer of the bare cluster, as obtained in the case of $n=13$. The study of the charge density and the density of states indicates that the HOMO-LUMO gap is increased through rearrangement of states upon passivation. It is observed that the optical gap generally decreases with an increase in the cluster size, though there are oscillations due to quantum confinement. The trend of the optical gap with increasing size suggests an underestimation of the optical gap within LDA, which is generally expected. Accordingly, we can say that an extrapolated optical gap to a size of 15 Å and more, is comparable to the experimental observation.

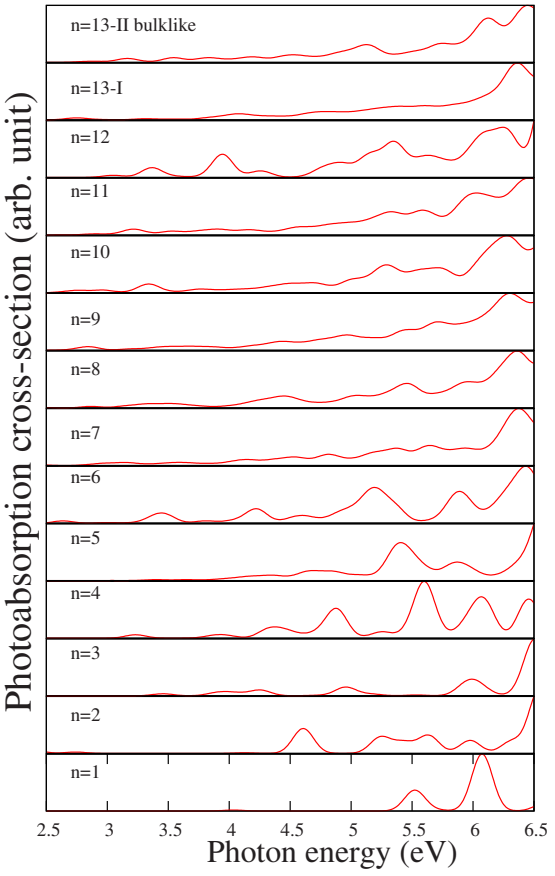

FIG. 7. (Color online) TD-LDA optical absorption spectra of the bare Zn_nSe_n ($n=1$ to 13) clusters. The spectra were convoluted with a Gaussian of standard deviation 0.1 eV.

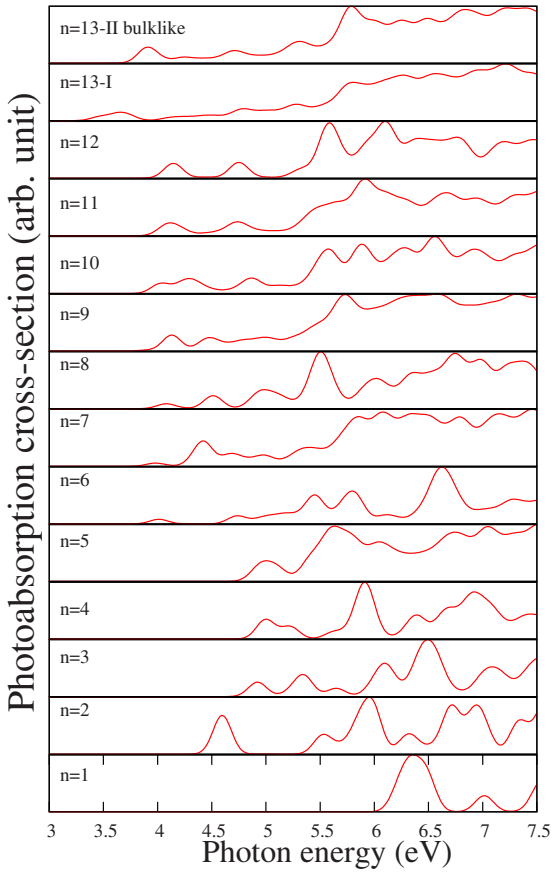

FIG. 8. (Color online) TD-LDA optical absorption spectra of the passivated Zn_nSe_n ($n=1$ to 13) clusters. The spectra were convoluted with a Gaussian of standard deviation 0.1 eV.

ACKNOWLEDGMENTS

The authors would like to thank C-DAC for the funding and the computing time on its PARAM series of supercomputers. V.K. gratefully acknowledges support from the U.S. Asian Office of Aerospace Research and Development. Helpful discussions with V. Nikesh, A. Lad, S. Chakraborty, and Ch. Rajesh are thankfully acknowledged. One of us (S.P.N.), would like to acknowledge the scientific discussions with I. Vasiliev and M. Tiago. The authors also thank J. R. Chelikowsky for providing PARSEC and TD-LDA code.

*svg@electronics.unipune.ernet.in

[1] A. P. Alivisatos, Science **271**, 933 (1996).
[2] M. G. Bawendi, V. C. Sundar, and F. V. Mikulec, U.S. Patent No. 6855551 (pending).
[3] I. L. Medintz, H. Tetsuouyeda, E. R. Goldman, and H. Mattoussi, Nature Mater. **4**, 435 (2005).
[4] X. Michalet, F. F. Pinaud, L. A. Bentolila, J. M. Tsay, S. Doose, J. J. Li, G. Sundaresan, A. M. Wu, S. S. Gambhir, and S. Weiss, Science **307**, 538 (2005).
[5] P. Reiss, New J. Chem. **31**, 1843 (2007).
[6] V. V. Nikesh, A. D. Lad, S. Kimura, S. Nozaki, and S. Mahamuni, J. Appl. Phys. **100**, 113520 (2006).
[7] A. D. Lad and S. Mahamuni, Phys. Rev. B **78**, 125421 (2008).
[8] J. M. Matxain, J. M. Mercero, J. E. Fowler, and J. M. Ugalde, Phys. Rev. A **64**, 053201 (2001).
[9] P. Deglmann, R. Ahlrichs, and K. Tsereteli, J. Chem. Phys. **116**, 1585 (2002).
[10] B. Goswami, S. Pal, P. Sarkar, G. Seifert, and M. Springborg, Phys. Rev. B **73**, 205312 (2006).
[11] B. Goswami, S. Pal, and P. Sarkar, Phys. Rev. B **76**, 045323 (2007).
[12] G. Kresse and J. Furthmüller, Phys. Rev. B **54**, 11169 (1996).
[13] G. Kresse and J. Furthmüller, Comput. Mater. Sci. **6**, 15 (1996).
[14] P. E. Blöchl, Phys. Rev. B **50**, 17953 (1994).
[15] G. Kresse and D. Joubert, Phys. Rev. B **59**, 1758 (1999).
[16] J. P. Perdew, K. Burke, and M. Ernzerhof, Phys. Rev. Lett. **77**, 3865 (1996).
[17] N. Kosugi, J. Comput. Phys. **55**, 426 (1984).
[18] A. Kasuya, R. Sivamohan, Y. A. Barnakov, I. M. Dmitruk, T. Nirasawa, V. R. Romanyuk, V. Kumar, S. V. Mamykin, K. Tohji, B. Jeyadevan, K. Shinoda, T. Kudo, O. Terasaki, Z. Liu, R. V. Belosludov, V. Sundararajan, and Y. Kawazoe, Nature Mater. **3**, 99 (2004).
[19] S. K. Bhattacharya and A. Kshirsagar, Phys. Rev. B **75**, 035402 (2007).
[20] S. K. Bhattacharya and A. Kshirsagar, Eur. Phys. J. D **48**, 355 (2008).
[21] X. Huang, E. Lindgren, and J. R. Chelikowsky, Phys. Rev. B **71**, 165328 (2005).
[22] M. M. G. Alemany, M. Jain, L. Kronik, and J. R. Chelikowsky, Phys. Rev. B **69**, 075101 (2004).
[23] J. R. Chelikowsky, N. Troullier, and Y. Saad, Phys. Rev. Lett. **72**, 1240 (1994).
[24] N. Troullier and J. L. Martins, Phys. Rev. B **43**, 1993 (1991).
[25] D. M. Ceperley and B. J. Alder, Phys. Rev. Lett. **45**, 566 (1980).
[26] J. P. Perdew and A. Zunger, Phys. Rev. B **23**, 5048 (1981).
[27] I. Vasiliev, S. Öğüt, and J. R. Chelikowsky, Phys. Rev. B **65**, 115416 (2002).
[28] W. R. Burdick, Y. Saad, L. Kronik, I. Vasiliev, M. Jain, and J. R. Chelikowsky, Comput. Phys. Commun. **156**, 22 (2003).
[29] J. R. Chelikowsky, J. Phys. D **33**, R33 (2000).